The influence of freeze–thaw cycles on the shear strength of illite clay

Steiner, A.; Vardon, Phil; Broere, Wout

DOI
10.1680/jgeen.16.00101

Publication date
2017

Document Version
Accepted author manuscript

Published in
Proceedings of the Institution of Civil Engineers - Geotechnical Engineering

The influence of freeze-thaw cycles on the shear strength of Illite clay

Author 1
- Amy Steiner, MSc
- Faculty of Civil Engineering and Geosciences, Section of Geo-Engineering, Delft University of Technology, Delft, the Netherlands

Author 2
- Philip J. Vardon, PhD (corresponding author)
- Faculty of Civil Engineering and Geosciences, Section of Geo-Engineering, Delft University of Technology, Delft, the Netherlands

Author 3
- Wout Broere, PhD, MSc
- Faculty of Civil Engineering and Geosciences, Section of Geo-Engineering, Delft University of Technology, Delft, the Netherlands

Full contact details of corresponding author.
Dr. Philip J. Vardon
Faculty of Civil Engineering and Geosciences
Delft University of Technology
P.O. Box 5048, 2628 CN Delft
the Netherlands
email: P.J.Vardon@tudelft.nl

Date written: June 2016, Revised February 2017, Re-revised May 2017

Number of words: 4034
Number of tables: 1
Number of figures: 12

Abstract (192 words)

Geo-energy infrastructure, such as ground source heat systems (thermo-active structures), induce thermal cycles that can result in changes of the bearing capacity of soil by changing, for example, the void ratio, soil structure, unit weight and hydraulic conductivity. The influence of repeated freeze/thaw (FT) cycles and different freezing rates on the shear strength of a frost susceptible Illite clay was investigated. Samples were subjected to between 1 and 20 FT cycles, and the shear strength of the thawed material was determined using undrained unconsolidated triaxial tests. After the shear strength decrease due to the first FT cycle, a transitory shear strength recovery occurred between 1 and 3 freezing cycles, followed by a shear strength decrease between 3 and 7 FT cycles, which then approached an equilibrium value. CT scans showed ice lenses increased in size moving away from the freezing surface, and more uniform ice distribution with increasing FT cycles. Changing the freezing rate yielded differences in the formation and structure of ice lenses perpendicular to the freezing direction. The observed failure plane typically coincides with the plane of the largest ice lens due to formation of a slurry layer after thawing.

Keywords chosen from ICE Publishing list

Strength & testing of materials, Thermal effects, Geotechnical engineering

List of notation

E	elastic modulus (stiffness) of the thawed soil
PI	Plasticity Index of the soil
PL	Plastic Limit of the soil
R	thermal resistance
T_{bf}	applied freezing temperature at the bottom of the sample
T_{bt}	applied thawing temperature at the bottom of the sample
e	void ratio
k	hydraulic conductivity
p	pore pressure
w	water content of the soil by mass
γ_d	dry unit weight

1. Introduction

Geo-energy infrastructure, such as ground source heat systems (thermo-active structures), induce thermal cycles that result in changes in bearing capacity by changing the void ratio, unit weight, hydraulic conductivity, and soil structure (Andersland and Ladanyi, 1994). Changes in the shear strength due to seasonal freezing and thawing (FT) cycles, as well as changes in thermal equilibrium of the soil due to construction, present challenges when engineering in cold regions. Cyclic thermal loads can be transferred into the ground by energy infrastructure, such as thermosiphons, energy piles, storage tanks, or pipelines, many of which can serve an additional structural function in cold regions. The changes in the physical properties of a soil during freezing and thawing alter the heat storage capacity of the soil, and design guidelines for thermal piles identify hydraulic conductivity as a major design factor (GHSPA, 2012).

The temperature at the soil surface, the type/properties of the soil, and the confining pressure influence the speed that the freezing front, defined as the boundary between frozen and unfrozen soils, penetrates the soil. Soil is considered frozen when the temperature is below 0ºC, even if the soil is dry and no ice is present (Talamucci, 2003).

When designing on clay, the undrained shear strength is often used as the primary design parameter, as it is the worst-case scenario (Vardanega and Bolton, 2011). Current design practices for engineering in frost susceptible soils focus on surface deformation caused by frost heaving, but changes in the soil structure due to repeated FT cycles may be deserving of greater consideration, as they result in long-term changes to soil strength. The freezing rate will influence the development of shear strength by altering the soil structure via formation of ice lenses. Strength evolution over multiple freeze thaw cycles can be evaluated using mobilised shear strength, defined as the shear stress in a medium which corresponds to the failure or deformation plane at a certain strain, i.e. the strength that is used or 'mobilised' (Ching and Phoon, 2013). The critical strength is when the material is in the unfrozen state, as the frozen pore water contributes considerably to shear strength (and stiffness).

FT cycles in clay have been observed to result in a reduction in shear strength, attributed to formation of large cracks, destruction of the soil's microstructure due to volumetric expansion of water during freezing, and formation of a saturated 'slurry' layer along the plane of the largest ice lens in the thawed material (Wang et al., 2007). The formation of this slurry layer results in a temporary decrease in shear strength, known as thaw weakening, until the water is able to redistribute back into the soil. Research has found that the largest change in shear strength occurs within the first 7 FT cycles, after which the strength stabilises (Qi et al., 2006).

Ice lenses are formed by two contributing factors: (1) the expansion of water as it turns to ice, and (2) water flowing towards horizontal ice layers, often through vertical cracks forming perpendicular to the freezing front. This water flow is primarily caused by negative pore pressures in the soil caused by the interface tension between ice and water in the region where the soil which is partially frozen, i.e. the frozen fringe, known as cryogenic suction (Thomas et al., 2009). Cracks form when the soil reaches its tensile strength, driven by either increases in pore pressure for the horizontal cracks for a vertical heat flow (Thomas et al., 2009), or by tensile stresses driven by water leaving the matrix for the vertical cracks. The vertical cracks, therefore, form below the horizontal lenses. With slower freezing rates, both vertical and horizontal cracks are larger, as water has longer to flow before the freezing front moves down. At higher freezing rates, water has less time to move through the soil and the resulting cracks are smaller. The development of temperature with depth, pore pressure distribution, and cryogenic suction distribution are schematised in Figure 1 for a soil with a freezing/thawing surface at the ground surface. In Figure 1(A), a soil profile is shown with the frozen zone shown in region (a), the frozen fringe and ice lens formation, where both frozen and liquid water exist, shown in region (b), and the unfrozen zone in region (c). In Figure 1(B), the temperature profile is schematised in a freezing condition, where the highest gradient is shown in the frozen zone due to the applied temperature (not steady state conditions) and the highest thermal conductivity. In Figure 1(C), the pore pressures are shown, with an ice lens forming at the highest pore pressure (above the tensile strength of the material). Figure 1(D) shows the variation of cryogenic suction, which occurs due to the interface stresses between the water and ice, therefore in the full frozen and fully unfrozen zones, cryogenic suction is 0 and increases from the edge of the frozen fringe towards the frozen zone.

This research evaluates the influence of different number of FT cycles and different freezing rates on the shear strength development and ice lens formation in an Illite clay (Steiner, 2016).

2. Methodology

A physical model setup has been developed for this research, which aims to evaluate the ice lensing and shear strength of undrained Illite clay subjected to one-dimensional freezing, in a closed system, where water cannot enter or leave.

Material and sample preparation

Samples were prepared in batches by mixing Illite clay (WBB Vingerling k122, with plastic limit (PL) = 23% and liquid limit (LL) = 57%, obtained from Deutschland (2016)) with water. The samples were prepared by adding water to the clay and mixing by hand until reaching the target water content, w, of ~34% and a dry unit weight, γ_d, of ~16.4 kN/m^3, yielding a void ratio of 0.62. The dry unit weight, water content and void ratio were determined for every prepared sample to ensure uniformity, with the details of the samples and the experiments undertaken with them given in Table 1. Samples were cut into 50 mm by 100 mm cylinders and the unit weight was measured for each sample. The samples where then placed into a water-tight membrane and secured to a copper plug with gaskets at the bottom end to prevent moisture loss during freezing and thawing. The frost susceptibility, which describes the tendency for ice segregation during freezing, of the clay was categorised as F3, using the USACE Frost Susceptibility Criteria (Chamberlain, 1981) based on the plasticity index (PI) of the soil (in this case PI = 34%, based on 3 tests). The samples were initially saturated, but became partially saturated due to water movement during the freezing process.

Experimental equipment and procedure

The freezing apparatus used in this research was developed by van den Bosch (2015), and is shown in Figure 2. The heat for freezing and thawing was provided via a Peltier element – a solid state thermo-electric device – which allows the conversion of electricity to a temperature gradient across the element. A Peltier element was used to allow fast and accurate temperature control. The base of the Peltier element was cooled (freezing) / heated (thawing) using a liquid cooled heat sink and cooling fan. The copper plug at the bottom of the sample, with an embedded temperature sensor that measures the temperature of the Peltier element, was used to transfer heat from the Peltier element to the soil. Temperature readings are also taken at the top of the sample via the temperature sensor at the top of the figure.

The samples were placed in an insulated container (Figure 3), placed directly onto the freezing/thawing equipment, and subjected to FT cycles. The insulation consisted of a 194 mm x 194 mm x 120 mm (l x w x h) box and a 60 mm x 50 mm (l x d) thick insert composed of URSA XPS insulation with a minimum thermal resistance R = 2.0 (m^{2}K)/W. The equipment was located in a temperature controlled laboratory, with the temperature controlled at 14.5°C ±1°C and humidity controlled at 70%. The sample was sealed at the base so water could not drain and the surrounding membrane extended at the top, so water could move to the top of the sample, but not leave the sample casing. Evaporation at the top of the sample was limited due to the cool air temperature and high humidity in the room, as well as the USRA XPS insulation insert placed above the sample.

The temperature was controlled at the base of the samples and fixed during freezing or thawing (T_{bf} during freezing, T_{bt} during thawing). The samples were considered completely frozen when the temperature at the top was below -2.5°C for at least 1 hour and completely thawed when the temperature at the top exceeded 3°C for 1 hour. The base temperature and number of cycles were controlled automatically via a computerised control system.

After the specified number of FT cycles, the still-frozen samples were placed in a triaxial testing machine and the loading piston was lowered (docked) and the triaxial cell was filled with 17°C water. The sample was allowed to thaw for at least 6.5 hours, then the water was replaced by de-aired 14.5°C water. The triaxial setup used is specifically calibrated for use on extremely soft samples and is based on a standard 50 kN GDS load frame, a STALC9-1kN load cell and 3 MPa controllers, recalibrated for low stress. For test ranges below 600 kPa the accuracy of the setup is rated < 0.17 kPa for axial stress, < 0.5kPa for cell pressure and < 0.2% for axial strain. Unconsolidated Undrained (UU) triaxial tests (strain controlled) in accordance with ASTM D2850-15: Standard Test Method for Unconsolidated Undrained Triaxial Compression Test for Cohesive Soils (ASTM,

2015), were undertaken to determine the shear strength of the thawed samples at a confining pressure of 400 kPa and a loading rate of 0.1 mm/min. In addition to the considerations given in the introduction of the critical strength in unfrozen conditions, the laboratory setup has not been calibrated for the significantly higher stress range that would be encountered in frozen samples, it was not considered appropriate to test frozen samples. Macro-Computerised Tomography (CT) scans using a Siemens SOMATOM Definition macro-CT scanner, were performed on some of the frozen samples to evaluate the changes in soil structure. UU triaxial tests (strain controlled) were done on never-frozen samples from each batch to obtain a reference shear strength and verify the initial variability of the material.

Experimental series

Two experimental series were undertaken:

- The first, to investigate the number of FT cycles, with 1, 3, 5, 7, 10, and 20 FT cycles with a T_{bf} = -20°C and a T_{bt} = 20°C.
- The second, to investigate the freezing rate, with a single FT cycle with applied freezing surface temperatures T_{bf} of -5, -10, -15, and -20°C (and T_{bt} = 20°C).

3. Results

Number of FT cycles

The strength development with axial strain for samples subjected to different FT cycles is shown in Figure 4. Test results were not corrected for membrane stiffness effects. Samples subjected to freezing all exhibited a significant reduction in shear strength compared to samples that have never been frozen. After a single FT cycle, the samples show a clear peak shear strength and subsequent softening behaviour. The samples also exhibit a greater initial stiffness, almost double that of the intact, never-frozen, sample, which is in agreement with existing literature. After the first FT cycle, the stiffness decreases at a diminishing rate, approaching an equilibrium stiffness after many cycles. At 3 FT cycles the sample is about half as stiff as a never-frozen sample, and exhibits strain hardening and shear strength recovery. At 7 to 10 FT cycles, similar behaviour is observed, the samples are weaker in shear strength than 3 FT cycles, stronger than 1 FT cycle (at high axial strains), strain harden and are less stiff than 1 or 3 FT cycles. After 7 FT cycles, the ice lens distribution through the sample stabilised and the stiffness increased. At 20 FT cycles, the initial behaviour matches that of 10 FT cycles, but a rapid transition to a residual shear strength occurs (similar to that from 1 FT cycle) with no softening or hardening. From this single 20 FT cycle test, however, the possible variation in residual shear strength cannot be reliably established. The soil stiffness decreased over the period where most of the structural changes within the soil occurred.

The same results are plotted in Figure 5 in terms of shear strength against number of FT cycles. As many of the samples strain harden, there is no peak shear strength to plot, therefore the mobilised shear strength at 2, 4, 6 and 10% axial strain have been shown. It is shown that after a substantial initial strength loss with a single FT cycle, strength recovery occurs between 1 and 3 FT cycles, which again reduces until 7 FT cycles.

Figure 6 shows photographic and CT scan images of the samples with different FT cycles. All samples show ice lenses which are primarily vertically oriented. The samples show a decrease in density and an increase in size of the ice lenses with increasing distance from the freezing side (the base). This is likely due to a decreasing thermal gradient due to temporal heat changes and lateral heat losses. As the number of FT cycles increases, the size of the ice lenses decreases in all locations in the sample. At 7 FT cycles onwards there are no perceivable differences between the samples. Moreover, with increasing cycles, the ice lens distribution becomes increasingly uniform over the height of the sample.

Freezing rate

Figure 7 presents the mobilised shear strength against axial strain for the second results series, different freezing rates, controlled by differing base freezing temperatures. Slower freezing rates, associated with warmer freezing

surface temperatures, resulted in lower shear strengths. A significant reduction in shear strength occurs between T_{bf} = -5°C and -10°C. The difference in shear strength and stiffness between -10°C and -15°C is much smaller.

The photographic and CT scan images with different freezing rates for this experimental series are presented in Figure 8. Horizontal ice lenses are visible for all samples frozen with T_{bf} < -20°C. Samples with slower freezing rates exhibited larger cracks and lensing in both horizontal and vertical directions. With faster freezing rates, smaller cracks/lenses were observed. Again, both vertical and horizontal cracking increased in size and decreased in amount moving away from the freezing side for all freezing rates. With decreasing T_{bf}, the ice lens distribution became more uniform. This was attributed to pore water freezing in place before water was able to flow due to cryogenic suction, thus preventing formation of bulk ice and reducing macro structural rearrangement.

With slow freezing rates (e.g., T_{bf} = -5°C), consolidation occurred at the top of the sample (furthest from the freezing side). This can be observed from the gap between the sample casing and sample (e.g., Figure 8a) above the large ice lens. The sample frozen with T_{bf} = -5°C exhibits almost no lensing in the top 25 mm of the sample. This was due to water movement towards the freezing front causing the soil to reach its shrinkage limit.

The location of the largest ice lens and failure plane for a subset of the samples are shown in Figure 9. The failure planes are seen to generally coincide with the plane of the largest ice lens. The thicker ice lenses at warmer freezing surface temperatures resulted in lower shear strength. This is attributed to the formation of the slurry layer when the sample is completely thawed and cannot drain or redistribute through the soil.

4. Analysis and discussion

4.1 Strength Behaviour

The intermediate strength recovery seen between 1 and 3 FT cycles (in the first experimental series) was not identified in existing literature. An almost continuous slurry layer along the plane of a horizontal ice lens occurred after 1 FT cycle. This lens is substantially smaller than observed in e.g. Figure 8a, and cannot be easily observed in Figure 6a but is identified in Figure 9d, alongside the failure plane on the failed sample. At 3 cycles, no continuous horizontal ice lens is visible, and therefore no slurry layer formed, resulting in a higher mobilised shear strength. After the first FT cycle, the space between the soil particles reduced during thawing, resulting in slight consolidation. The lack of a continuous horizontal ice lens at 3 FT cycles explains the strength recovery between the first and third FT cycles. The presence of strain hardening and residual strain for samples subjected to more than 1 FT cycle indicates the material can carry larger loads before failing in the range of strength measured. Strain softening was only seen after 1 freezing cycle, and was not identified as a phenomena in existing literature. The strain softening after 1 FT cycle suggests a significant amount of damage occurs during the first freezing cycle, and can be attributed to the onset of clay fragmentation that occurs as the sample cracked during freezing.

Thicker ice lenses resulted in lower shear strengths, due to continuous ice lenses, and after thawing, porewater is unable to redistribute in to the soil due to very low gradients and decreased permeability due to consolidation of the clay. Lower freezing gradients (in this case, from warmer fixed freezing temperatures) approaching 0°C result in larger ice lenses and therefore weaker soils. Based on these results, locally freezing clay as a stabilisation measure in construction would be best done using a colder freezing temperature for more rapid freezing.

An attempt was made to investigate the repeatability and variability of the impact of freeze thaw cycles by repeating tests with all the same conditions. Freezing and consequential cracking added additional variability into the samples as the crack patterns are strongly influenced by local imperfections. However, the repeatability is significant, as seen in Figure 4, although differences are clear between samples. Therefore, the local variabilities observed are not significant at the element level in terms of describing the qualitative processes and behaviour. Overall, the never-frozen samples had a maximum variability from the mean of approximately 16% (10 samples), while the variation from the mean of thawed samples was approximately 13% (15 samples). Given the heterogeneous nature of soil, this indicates that the sample preparation and testing was sufficiently consistent. The true reliability of the results is difficult to determine, as there are insufficient data points to assess the error and develop a standard deviation. More tests are needed to draw conclusions about the reliability

and variation within the samples, especially between 1 and 3 FT cycles, where the results were not as expected based on the literature review and models. Test results were also not corrected for membrane stiffness effects, which would affect the quantitative values reported, but not the qualitative trends.

4.2. Ice lens formation

It can be seen in Figures 8 and 9 that slower freezing rates result in larger ice lenses, which allows formation of slurry layers and a consequential weak plane in the soil. This discontinuity results in decreased shear strength and reduced stiffness compared to the never-frozen material. Samples frozen with T_{bf} = -5°C exhibited almost no lensing in the top 25 mm of the sample, but had a very large ice lens. The lack of ice lensing in the upper portion of the sample is attributed to movement of pore water towards the freezing front and active ice lens via cryogenic suction until the 'unfrozen' soil reached its shrinkage limit. At this point, the soil could desaturate and any remaining water could mostly freeze within the pore space, therefore not causing any significant fracturing or cracking of the soil. The pore water in the thawed sample along the plane of the slurry layer will try to redistribute through the sample, due to excess pore pressures derived from the consolidated material above, but, due to the sealed nature of the samples drainage out of the sample was not possible. Moreover, the soil fragments will have become consolidated, and will not swell to the same initial volume, therefore it is likely that there will be some free water/slurry in the sample.

Formation of many, small ice lenses destroys the soil microstructure and results in a reduction of shear strength. The presence of larger ice lenses with slower freezing rates results in significant weakening under undrained conditions due to formation of a saturated zone that acts as a failure plane. The equilibrium shear strength reached when T_{bf} < -10°C coincides with fewer changes in the soil structure. The difference in ice lens formation between T_{bf} = -15°C and T_{bf} = -20°C is significantly less than the difference between T_{bf} = -5°C and T_{bf} = -10°C. The increasingly uniform ice lens distribution with increasing freezing rate is caused by pore water freezing rapidly and a reduced influence of cryogenic suction. Similarly, changes in ice lens distribution decrease dramatically between 1 and 3 FT cycles, and are more similar between 5 and 7 cycles. After 7 cycles, the ice lens distribution stabilised, along with the shear strength. This is in agreement with research by Ghazavi and Roustaei (2013), Arenson et al. (2008), and Konrad (1998).

4.3. Stiffness

The development of soil stiffness with increasing FT cycles is given in Figure 10. The stiffness after 1 FT cycle at T_{bf} = -20°C is almost double that of never-frozen soil. Hypothetically, continuing to increase the freezing rate by lowering the surface freezing temperature could result in greater stiffness. This increased stiffness after 1 FT cycle may be due to the soil fragments consolidating locally during the first freezing cycle. This phenomenon has been documented by Volokhov (2003), Ghazavi and Roustaei (2013), Qi et al. (2008) and Simonsen and Isacsson (2001). With increasing FT cycles, the microstructure is rapidly destroyed, resulting in decreasing stiffness, for example at 3 FT cycles the stiffness is about a half of the original. The decrease is stiffness mainly occurs in the first few cycles. At low freezing rates, any local consolidation after the first freezing cycle is offset by the formation of large ice lenses that act as failure planes. The development of stiffness and mobilised shear strength with different freezing rates at 1 FT cycle is shown in Figure 11. For T_{bf} > -20°C, the stiffness is lower than that of a never-frozen sample.

The decreasing stiffness with decreasing freezing rate, seen in Figure 11, supports the considerations suggested by GHSPA (2012) for design of energy piles. This change in stiffness can be attributed to the fragmentation and destructuring of the clay, a faster freezing rate yields a less fragmented material thus structure and stiffness is maintained. The relationship between a softer (less stiff) soil and lower shear strength with decreasing freezing rates is not in agreement with the findings of Ghazavi and Roustaei (2013), who found an increase in stiffness approaching 0°C. This difference is attributed in part to the low confining pressures used in their research (between 30 and 90 kPa), as both stiffness and shear strength are known to increase with confining pressures. From Volokhov (2003), Simonsen and Isacsson (2001), and Qi et al. (2008), soil stiffness increases after the first freezing cycle, regardless of freezing rate, was expected to be larger than that of the never-frozen material. Instead, lower shear strengths seen with slower freezing rates correspond to lower stiffness. This was attributed

to the influence of the slurry layers that form along the plane of the largest ice lens and associated reduction in shear strength.

The development of mobilised shear strength with increasing FT cycles is shown in Figure 12. Between 3 and 7 FT cycles, both the shear strength and stiffness decrease. There is an increase in stiffness at 10 FT cycles that coincides with the equilibrium shear strength. The shear strength at 1 and after 10 FT cycles is approximately the same when the variability of the system is taken in to account.

4.4. Void Ratios

While the initial void ratio of the samples is uniform between samples and within the samples (Table 1), the void ratio is highly non-uniform in each sample after freezing (Figures 6 and 8). This means that the void ratio of the fragments would be significantly lower than as prepared, with the areas between these fragments having a very low void ratio. Due to the very small nature of these fragments, these have not been quantifiably measured. Based on the results of the CT scans, the void ratio of the intact fragments decreases as the soil microstructure degrades, and cracks appear. As the samples are frozen and porewater migration occurs, local consolidation occurs on the thawed side of the freezing front due to cryogenic suction, resulting in a smaller void ratio in the fragments. Samples exposed to more freezing cycles have increasingly more and smaller cracks, regaining therefore a more uniform void ratio as the microstructure degrades, and the changes in void ratio can be correlated to changes in soil strength and stiffness.

4.5. Scale effects

The tests done for this research are not true element tests and are therefore subject to scale effects. As seen in the CT scans and literature, formation of ice lenses is highly depth dependent and is a function of the temperature gradient, water availability and soil properties (e.g., compressibility, hydraulic conductivity). To capture the structural changes and ice distribution, large samples are needed. The time required for the entire sample to freeze or temperature at the top of sample to stabilise varied with applied surface temperature. The sample size used in this research was designed to be small enough that the freezing front would penetrate the entire sample and freeze all the pore water. An external water supply (excess water placed on top of the sample) would keep the material fully saturated and encourage more extensive ice lens formation. The lack of external water supply resulted in some of the soil exhibiting no ice lensing (e.g., Figure 9a at the top of the sample). The rate of freezing also varies with depth, due to the transience of the temperature boundary and heat losses from the sample edges (in the laboratory).

The strength recovery between 1 and 3 FT cycles, attributed to changes in ice lens formation and formation of a slurry layer, suggests that in cold regions, foundation elements are best constructed and allowed to experience at least 1 complete FT cycle before applying loads. Current construction practices in areas such as Alaska, often involve re-levelling or adjusting foundations after the first winter before completing the structure (Perreault, 2016). Allowing sufficient time between thawing and finishing constructions could allow the weak slurry layers along the ice lens planes to dissipate and the clay to regain some strength. The large reduction in shear strength at low axial strains (due to the increase in stiffness) after 1 FT cycle should be considered for engineering design, as the change in strength may be of greater influence than frost heaving. The undrained shear strength after 1 FT cycle should be used as a conservative design value, as application of surface loads will accelerate consolidation and result in a stronger soil in the long-term. If freezing clays as a soil stabilisation measure, applying a freezing surface temperature below -10°C will result in smaller ice lenses and a higher shear strength after thawing.

5. Conclusions

The shear strength of Illite clay reduced significantly after being exposed to freeze-thaw cycles. This behaviour is strongly affected by the rate of freezing and the number of cycles. Moreover the stiffness of the samples was seen to significantly change. After 1 FT cycle, the stiffness of the thawed sample with T_{bf} = -20°C was almost double that of a never-frozen sample, and failed at a low axial strain. Strength recovery was seen between 1 and 3 freezing cycles, along with a decrease in stiffness. The strength recovery was attributed to changes in the soil

structure due to formation of ice lenses, where a horizontal lens formed across the entire width of the sample after 1 FT cycle, which was not present at 3 cycles. With increasing FT cycles, the size of ice lenses in the soil decrease and the distribution over the sample height becomes increasingly uniform until an equilibrium condition is reached around 7 FT cycles. The shear strength equilibrium coincides with a stabilisation of the soil structure and stiffness.

As the freezing rate decreases, the shear strength and soil stiffness decrease. The largest change in shear strength occurred between T_{bf} = -5°C and -10°C, after which the shear strength continued to decrease at a diminishing rate approaching an equilibrium strength. This was observed to be due to the formation of large horizontal ice lenses, which are larger with greater temperatures. These lens formed a saturated slurry layer that acts as the primary failure plane in the thawed soil and caused a reduction in shear strength. However, it is noted that with different boundary conditions, different results would be yielded.

Additional research, varying the boundary conditions, confining pressures and drainage measuring the stiffness, cohesion, angle of internal friction, and void ratio with increasing FT cycles would provide further insight in to the relationship between these properties and shear strength development with freezing and thawing cycles.

Acknowledgements

The authors would like to acknowledge the help of Han de Visser, Kees van Beek and Marten van der Meer, whose help in the construction, trouble-shooting and execution of the experiments was invaluable.

References

ANDERSLAND, O. B. & LADANYI, B. 1994. *Introduction to Frozen Ground Engineering*, Chapman & Hall.

ARENSON, L. U., AZMATCH, T. F. & SEGO, D. C. 2008. A New Hypothesis on Ice Lens Formation in Frost-Susceptible Soils. *In:* KANE, D. L. & HINKEL, K. M. (eds.) *Ninth International Conference on Permafrost.* Fairbanks, Alaska: Institute of Northern Engineering.

ASTM 2015. Standard Test Methods for Unconsolidated-Undrained Traixial Compression Test on Cohesive Soils. D2850-15. ASTM.

VAN DEN BOSCH, T. J. H. 2015. *Influences of ice lens formation in silty soils.* MSc geo-engineering, Delft University of Technology.

CHAMBERLAIN, E. J. 1981. *CRREL Monograph 81-2 Frost susceptibility of soils*, USACE.

CHING, J. & PHOON, K. 2013. Mobilized shear strength of spatial variable soils under simple stress. *Structural Safety,* 41**,** 20-28.

DEUTSCHLAND, S. 2016. *Klei - G&S en Vingerling* [Online]. Available: http://www.creavisie.com/nl/content/klei-creaton-vingerling [Accessed 2016].

GHAZAVI, M. & ROUSTAEI, M. 2013. Freeze-thaw performance of clayey soil reinforced with geotextile layer. *Cold Regions Science and Technology,* 80**,** 22-29.

GHSPA 2012. Thermal pile design, installation and material standards. *In:* CENTER, N. E. (ed.). Davy Avenue, Knowlhill, Milton Keynes: National Energy Center.

KONRAD, J. M. 1998. Physical processes during freeze-thaw cycles in clayey silts. *Cold Regions Science and Technology,* 16**,** 291-308.

PERREAULT, P. V. 2016. *Altering the thermal regime of soils below heated buildings in the continuous and discontinuous permafrost zones of Alaska.* PhD, University of Alaska Fairbanks.

QI, J., MA, W. & SONG, C. 2008. Influence of freeze-thaw on engineering properties of a silty soil. *Cold Regions Science and Technology,* 53**,** 397-404.

QI, J., VERMEER, P. A. & CHENG, G. 2006. A Review of the Influence of Freeze-thaw Cycles on Soil Geotechnical Properties. *Permafrost and Periglacial Processes,* 17**,** 245-252.

SIMONSEN, E. & ISACSSON, U. 2001. Soil behavior during freezing and thawing using variable and constant confining pressure triaxial tests. *Canadian Geotechnical Journal* 38**,** 863-875.

STEINER, A. 2016. *The influence of freeze-thaw cycles on the shear strength of Illite clay.* MSc, Delft University of Technology.

TALAMUCCI, F. 2003. Freezing processes in porous media: Formation of ice lenses, swelling of the soil. *Mathematical and Computer Modelling,* 37**,** 595-602.

THOMAS, H. R., CLEALL, P., LI, Y. C., HARRIS, C. & KERN-LUETSCHG, M. 2009. Modelling of cryogenic processes in permafrost and seasonally frozen soils. *Geotechnique,* 59**,** 173-184.
VARDANEGA, P. J. & BOLTON, M. D. 2011. Strength mobilization in clays and silts. *Canadian Geotechnical Journal,* 48**,** 1485-1503.
VOLOKHOV, S. S. 2003. Effect of Freezing Conditions on the Shear Strength of Soils Frozen Together with Materials. *Soil Mechanics and Foundation Engineering,* 40.
WANG, D.-Y., MA, W., NIU, Y.-H., CHANG, Z.-X. & WEN, Z. 2007. Effects of cyclic freezing and thawing on mechanical properties of Qinghai-Tibet clay. *Cold Regions Science and Technology,* 48**,** 34-43.

Figure captions

Figure 1. Schematisation of soil behaviour: A) Soil profile; B) Temperature profile; C) Pore pressure profile; D) Cryogenic suction profile (based on Andersland and Ladanyi, 1994, and Arenson et al., 2008)
Figure 2. Schematic of freeze-thaw apparatus
Figure 3. Schematic of insulated sample container and actual container
Figure 4. Mobilised shear strength vs. axial strain for samples subjected to multiple FT cycles
Figure 5. Mobilised shear strength vs. number of FT cycles at different axial strains
Figure 6. CT scans for different numbers of FT cycle and T_{bf} = -20°C. TOP: Cracking on frozen sample before loading into triaxial cell; MIDDLE: CT scan of frozen sample. Pale grey is ice, white is soil, and black is voids; BOTTOM: Contrast CT showing ice distribution. White is solids, blue is ice, black is voids. (a) to (d) increasing FT cycles: 1, 3, 7, 10. (e) schematic showing freezing direction
Figure 7. Mobilised shear strength vs. axial strain for samples subjected to 1 FT cycle at different freezing rates
Figure 8. CT scans for 1 FT cycle at different freezing rates. TOP: Cracking on frozen sample before loading into triaxial cell; MIDDLE: CT scan of frozen sample. Pale grey is ice, white is soil, and black is voids; BOTTOM: Contrast CT showing ice distribution. White is solids, blue is ice, black is voids. (a) to (d): T_{bf} = -5, -10, -15, -20°C. (e) schematic showing freezing direction
Figure 9. CT scan of frozen samples with location of largest ice lens and failure plane after triaxial tests
Figure 10. Stiffness vs. number of freeze/thaw cycles
Figure 11. Stiffness vs. applied freezing temperature T_{bf}
Figure 12. Stiffness vs. mobilised shear strength for different number of FT cycles

Table captions

Table 1. Sample details and the experimental procedure they were used for.

Table 1. Sample details and the experimental procedure they were used for.

T_{bf} [°C]	# cycles	w [%]	γ_{dry} [kN/m^3]	e [-]
-20	1	34	16.18	0.61
-20	1	33	16.31	0.62
-20	3	34	16.54	0.62
-20	3	33	17.67	0.67
-20	5	36	15.85	0.60
-20	5	34	16.54	0.62
-20	7	35	16.18	0.61
-20	7	34	16.54	0.62
-20	10	35	16.19	0.61
-20	20	35	15.86	0.60
-15	1	33	16.51	0.62
-10	1	35	16.18	0.61
-10	1	33	16.51	0.62
-5	1	34	16.18	0.61

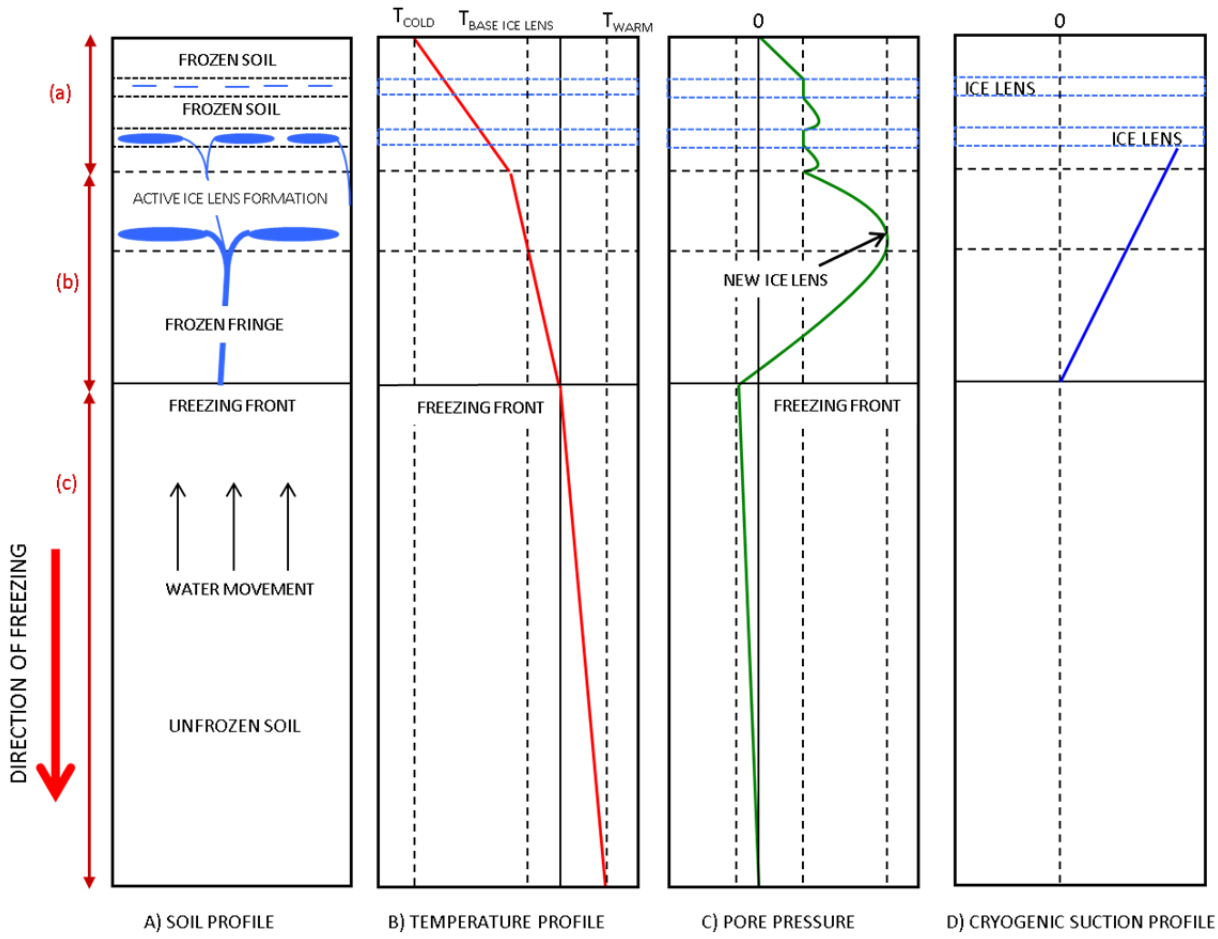

Figure 1. Schematisation of soil behaviour: A) Soil profile; B) Temperature profile; C) Pore pressure profile; D) Cryogenic suction profile (based on Andersland and Ladanyi, 1994, and Arenson et al., 2008)

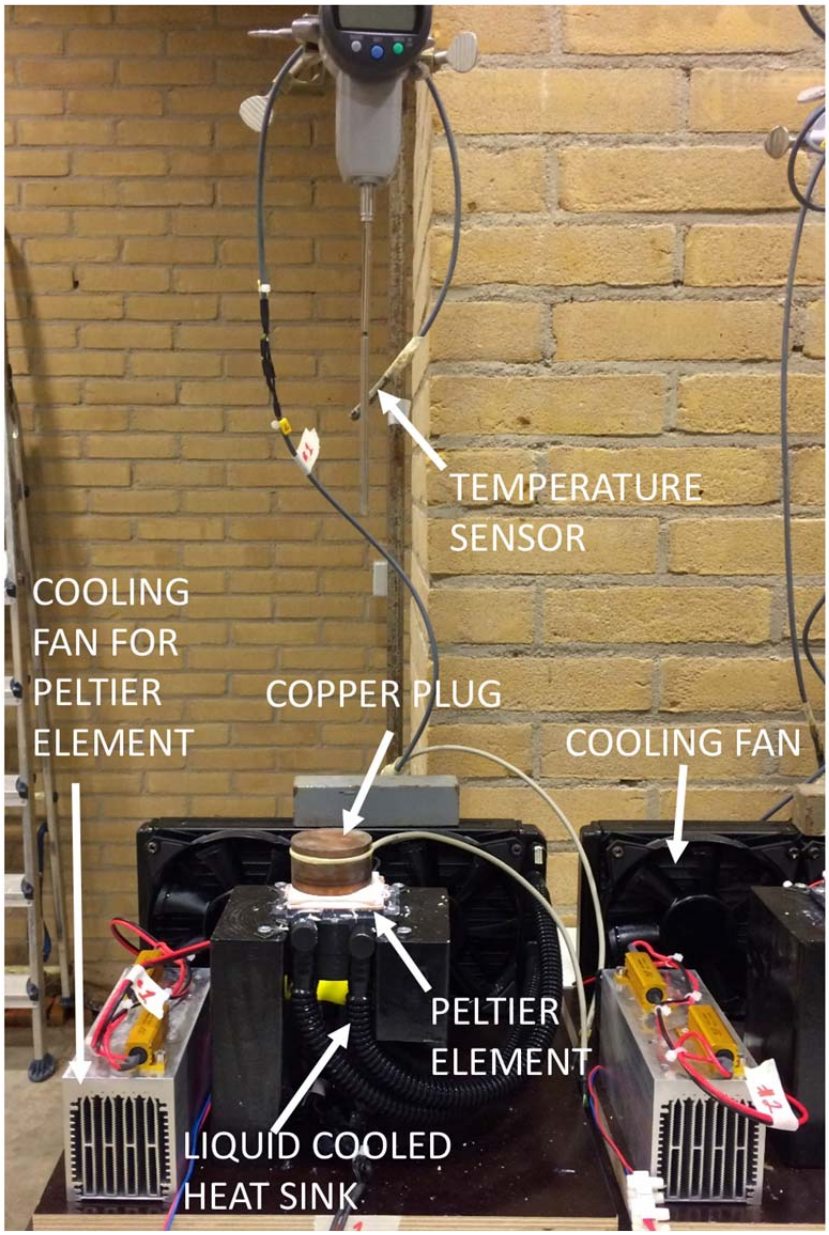

Figure 2. Schematic of freeze-thaw apparatus

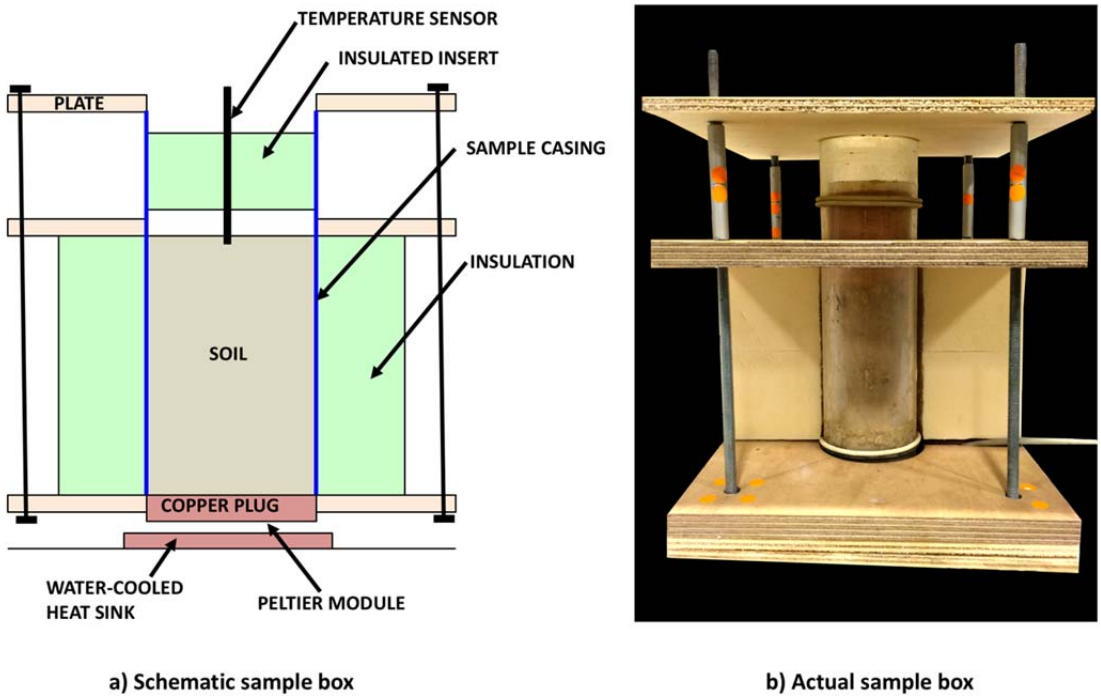

Figure 3. Schematic of insulated sample container and actual container

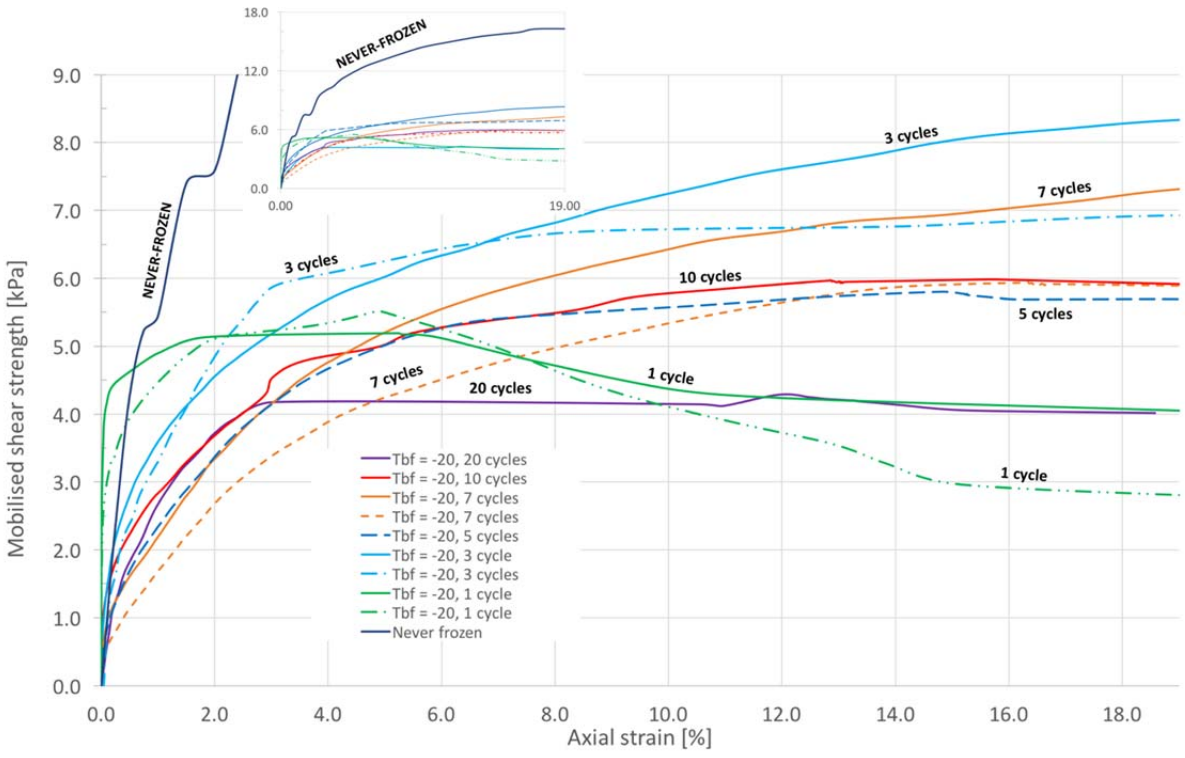

Figure 4. Mobilised shear strength vs. axial strain for samples subjected to multiple FT cycles

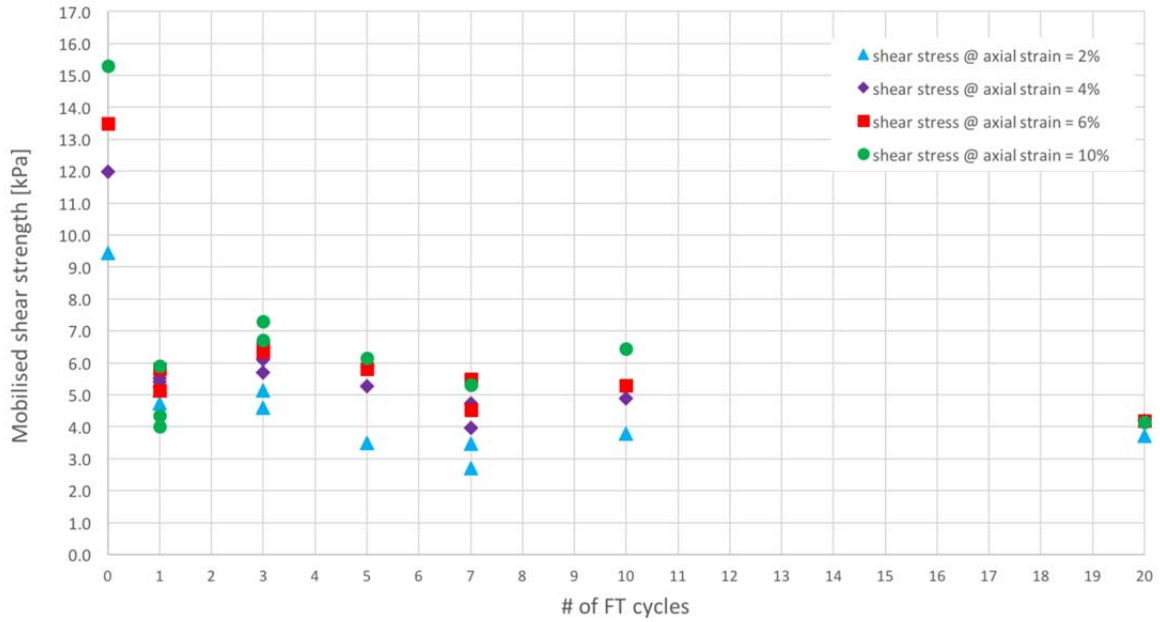

Figure 5. Mobilised shear strength vs. number of FT cycles at different axial strains

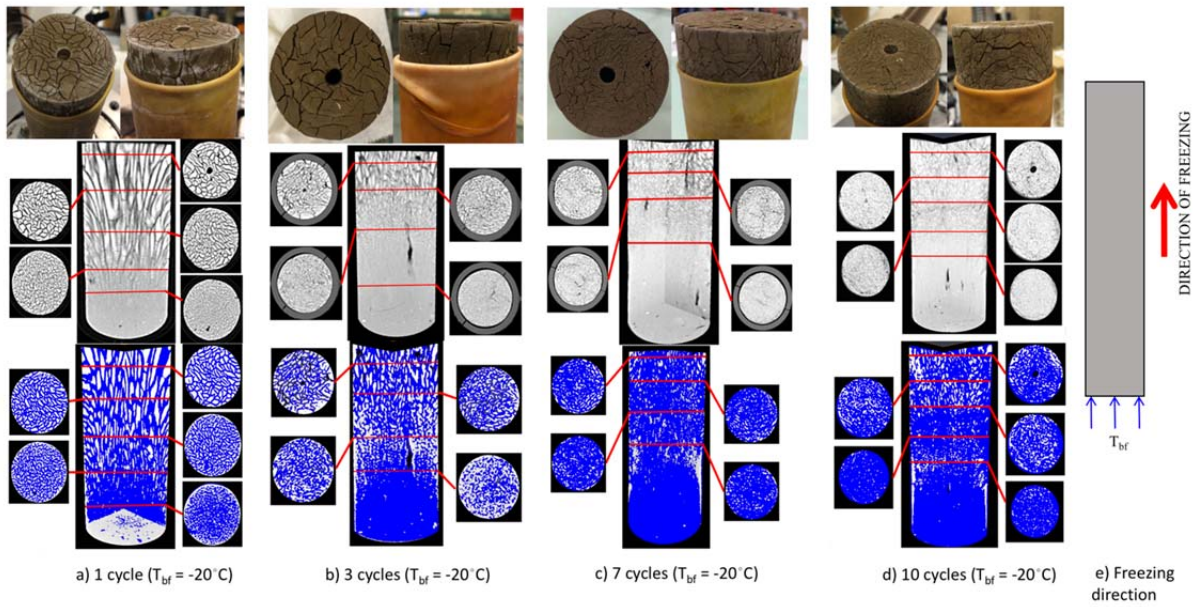

Figure 6. CT scans for different numbers of FT cycle and T_{bf} = -20°C. TOP: Cracking on frozen sample before loading into triaxial cell; MIDDLE: CT scan of frozen sample. Pale grey is ice, white is soil, and black is voids; BOTTOM: Contrast CT showing ice distribution. White is solids, blue is ice, black is voids. (a) to (d) increasing FT cycles: 1, 3, 7, 10. (e) schematic showing freezing direction

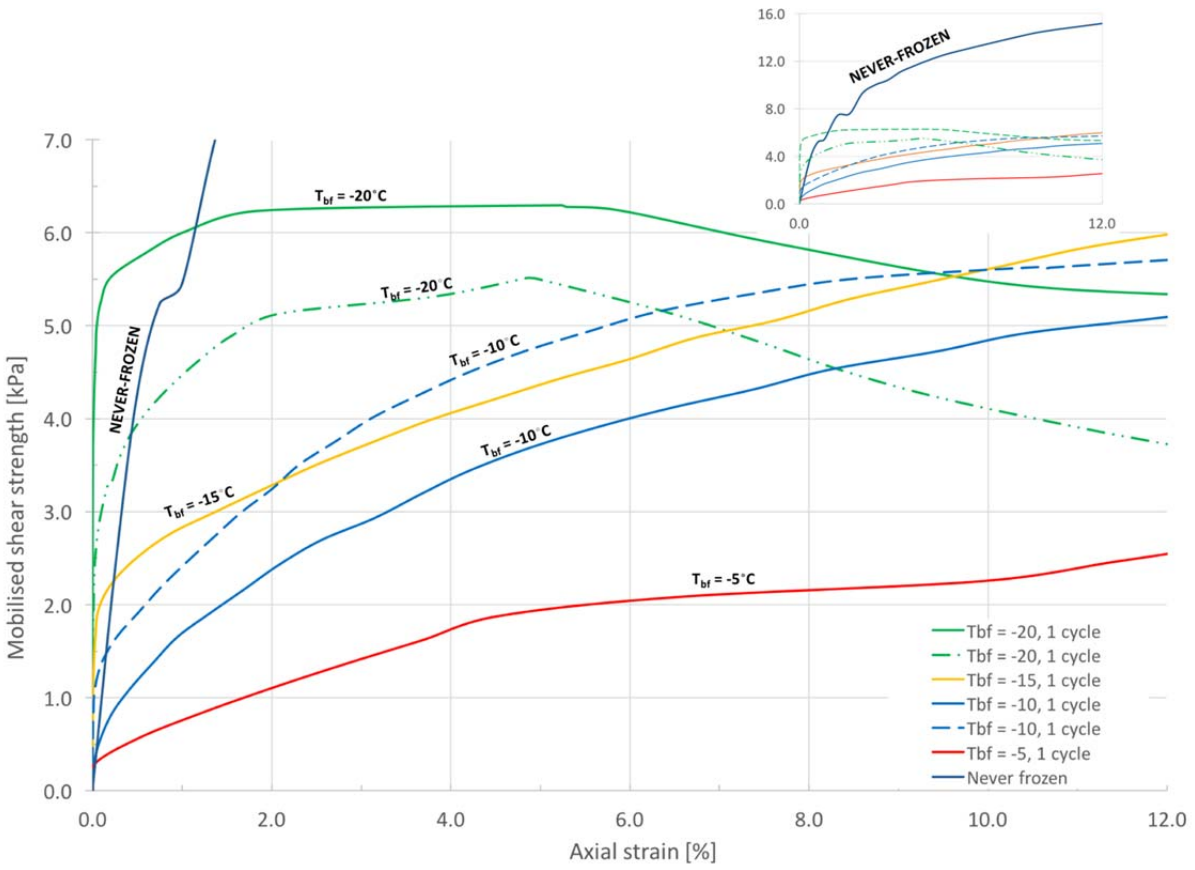

Figure 7. Mobilised shear strength vs. axial strain for samples subjected to one FT cycle at different freezing rates

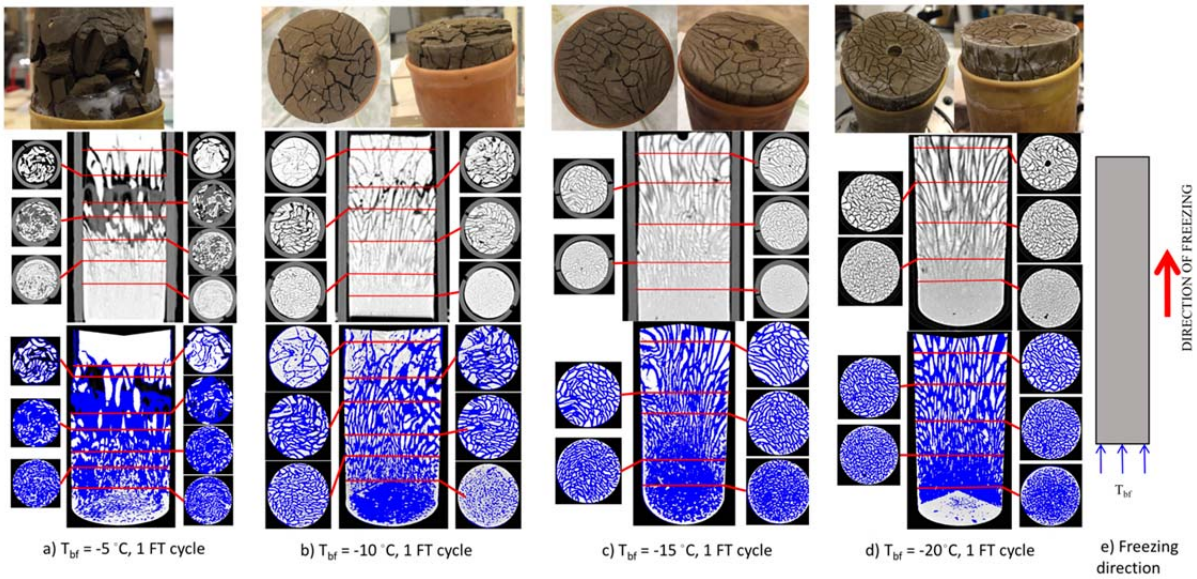

Figure 8. CT scans for one FT cycle at different freezing rates. TOP: Cracking on frozen sample before loading into triaxial cell; MIDDLE: CT scan of frozen sample. Pale grey is ice, white is soil, and black is voids; BOTTOM: Contrast CT showing ice distribution. White is solids, blue is ice, black is voids. (a) to (d): T_{bf} = -5, -10, -15, -20°C. (e) schematic showing freezing direction

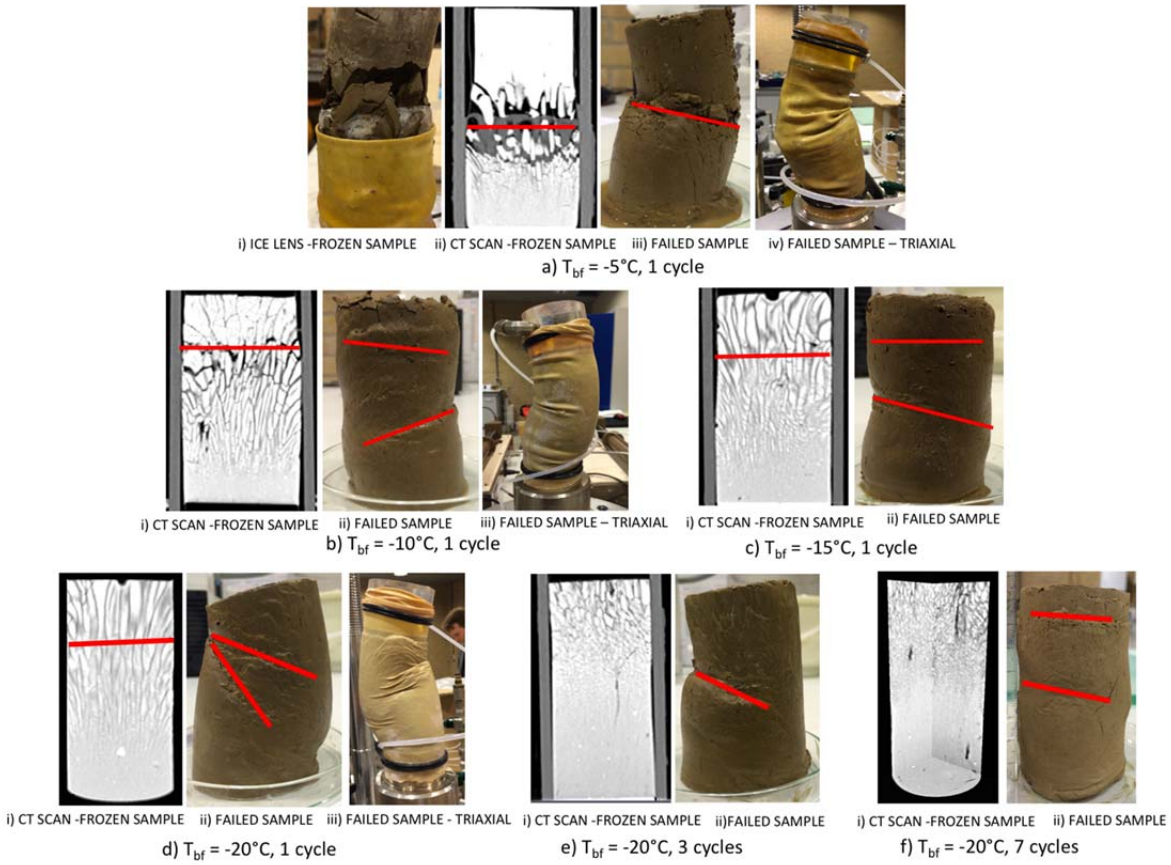

Figure 9. CT scan of frozen samples with location of largest ice lens and failure plane after triaxial tests

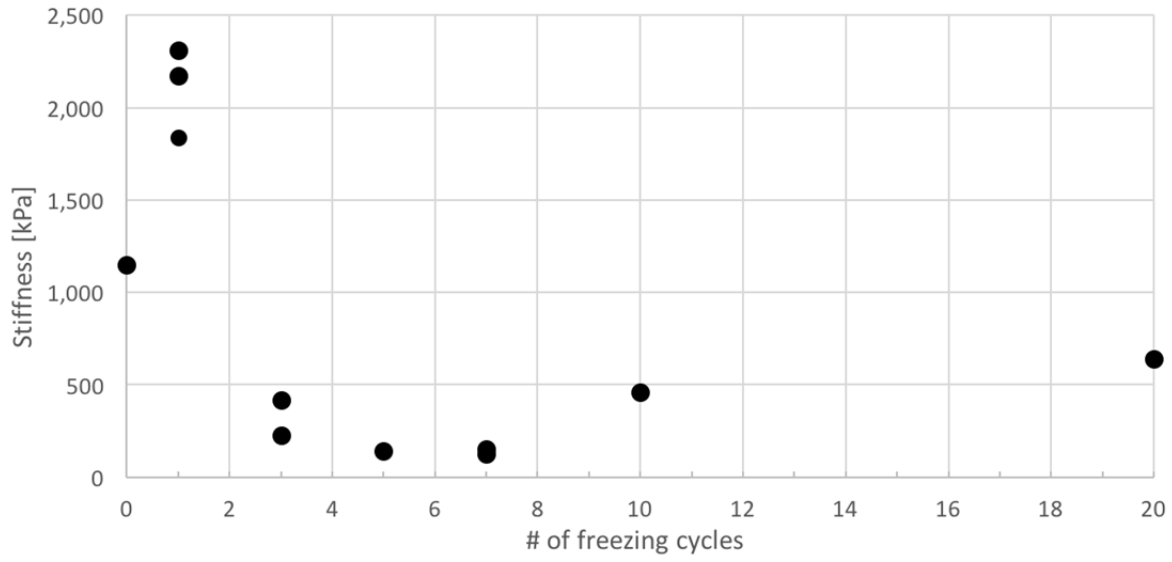

Figure 10. Stiffness vs. number of freeze/thaw cycles

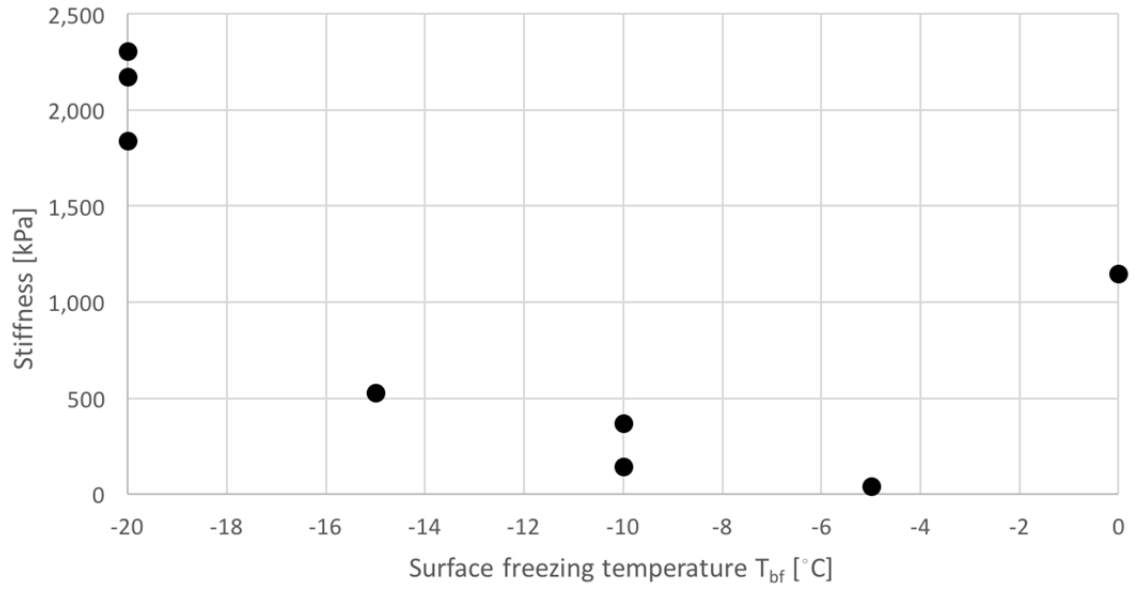

Figure 11. Stiffness vs. applied freezing temperature T_{bf}

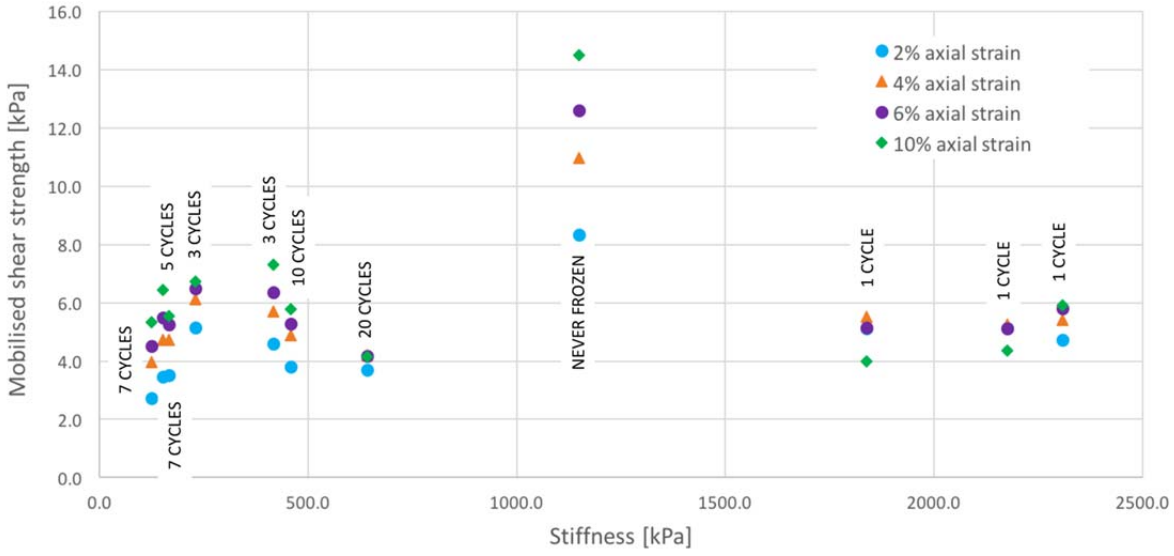

Figure 12. Stiffness vs. mobilised shear strength for different number of FT cycles